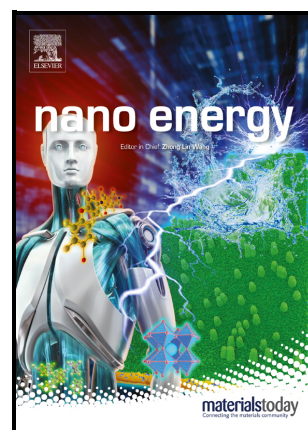


Indoor Organic Photovoltaic Module with 30.6% Efficiency for Efficient Wireless Power Transfer

Wenxuan Wang, Yong Cui, Yue Yu, Jianqiu Wang, Chaoyi Wang, Hao Hou, Qian Kang, Hui Wang, Shiyao Chen, Shaoqing Zhang, Haiping Xia, Jianhui Hou



PII: S2211-2855(24)00641-4

DOI: <https://doi.org/10.1016/j.nanoen.2024.109893>

Reference: NANOEN109893

To appear in: *Nano Energy*

Received date: 24 April 2024

Revised date: 12 June 2024

Accepted date: 14 June 2024

Please cite this article as: Wenxuan Wang, Yong Cui, Yue Yu, Jianqiu Wang, Chaoyi Wang, Hao Hou, Qian Kang, Hui Wang, Shiyao Chen, Shaoqing Zhang, Haiping Xia and Jianhui Hou, Indoor Organic Photovoltaic Module with 30.6% Efficiency for Efficient Wireless Power Transfer, *Nano Energy*, (2024)  
doi:<https://doi.org/10.1016/j.nanoen.2024.109893>

This is a PDF file of an article that has undergone enhancements after acceptance, such as the addition of a cover page and metadata, and formatting for readability, but it is not yet the definitive version of record. This version will undergo additional copyediting, typesetting and review before it is published in its final form, but we are providing this version to give early visibility of the article. Please note that, during the production process, errors may be discovered which could affect the content, and all legal disclaimers that apply to the journal pertain.

## Indoor Organic Photovoltaic Module with 30.6% Efficiency for Efficient Wireless Power Transfer

Wenxuan Wang<sup>1,2</sup>, Yong Cui<sup>1\*</sup>, Yue Yu<sup>1,2</sup>, Jianqiu Wang<sup>1</sup>, Chaoyi Wang<sup>3</sup>, Hao Hou<sup>4</sup>, Qian Kang<sup>4</sup>, Hui Wang<sup>5</sup>, Shiyan Chen<sup>5</sup>, Shaoqing Zhang<sup>3</sup>, Haiping Xia<sup>5\*</sup>, Jianhui Hou<sup>1,2,3\*</sup>

<sup>1</sup>State Key Laboratory of Polymer Physics and Chemistry, Beijing National Laboratory for Molecular Sciences, CAS Research/Education Center for Excellence in Molecular Sciences, Institute of Chemistry, Chinese Academy of Sciences, Beijing 100190, China

<sup>2</sup>University of Chinese Academy of Sciences, Beijing 100049, China

<sup>3</sup>School of Chemistry and Biology Engineering, University of Science and Technology Beijing, Beijing 100083, China

<sup>4</sup>College of Materials Science and Engineering, Beijing University of Technology, Beijing 100124, China

<sup>5</sup>Shenzhen Grubbs Institute and Department of Chemistry, Southern University of Science and Technology Shenzhen, Shenzhen 518055, China

\*Correspondence: [ycui1990@iccas.ac.cn](mailto:ycui1990@iccas.ac.cn); [xiahp@sustech.edu.cn](mailto:xiahp@sustech.edu.cn); [hjhzl@iccas.ac.cn](mailto:hjhzl@iccas.ac.cn);

**Keywords:** dicarbolong-phenanthroline, cathode interlayer, high efficiency, wireless power transfer, indoor applications

### Abstract

Organic photovoltaic (OPV) cells possess substantial advantages for indoor applications. However, the underdeveloped cathode interlayer hinders the industrialization of indoor OPV cells. Here, we introduce a phenanthroline derivative with weak nucleophilicity, dicarbolong-phenanthroline (DCP), as the cathode interlayer and comprehensively examine its utilization in indoor OPV cells. DCP exhibits thin depletion region width, which is beneficial for the charge extraction at the interface, thereby contributing to improved power conversion efficiency (PCE). Moreover, DCP presents high adaptability for coating process due to its thickness insensitivity. A DCP-based OPV module is fabricated by blade-coating method, reaching a high maximum

output voltage of 4.00 V and a remarkable PCE of 30.6% at 1000 lux. The OPV module can be successfully applied for efficient wireless power transfer. Furthermore, the DCP-based cell demonstrates outstanding device stability with a lifetime of 32000 hours under indoor lighting. These results demonstrate the promising potential of DCP-based OPV cells for indoor applications.

## 1. Introduction

Organic photovoltaic (OPV) cells incorporate the features of startup ability under weak illumination, tunable absorption spectrum, flexibility, absence of heavy metal and etc., presenting outstanding superiority for indoor applications [1-7]. OPV cells have achieved prominent power conversion efficiency (PCE) over 30% under indoor lighting, which fulfills the requirements of practical applications [8-11]. In order to further facilitate the industrialization of indoor OPV cells, excellent device stability, which involves the stability of active layer and interfacial layer, is quite critical. Previous literature has reported that the active layer has significant structural and morphological stability under mild indoor lighting conditions [10]. However, the stability of interlayer, particularly the cathode interlayer (CIL), remains a critical concern. The main reason is that many commonly used CIL materials possess alkalinity accompanied by nucleophilic groups, which likely damages the active layer and electrodes during the long-term operation of OPV cells, causing increased density of trap states [12-14]. Under weak illumination, the charge carrier density in OPV cells obviously decreases and trap-assist recombination dominates the charge recombination process [15-17]. The high density of trap states will cause severe charge recombination and thus depress the photovoltaic performance of indoor OPV cells. Therefore, developing CIL materials is significantly important for enhancing the device stability and promoting the practical applications of indoor OPV cells.

Since the chemical reaction between the active layer, interlayer and electrode is the main issue to restrict the stability of indoor OPV cells, the device stability can be expected to break through if the chemical reaction can be avoided. This demands that the CIL is free of alkalic

groups. Moreover, apart from the general properties, such as suitable energy level, high conductivity and high transmittance, the thickness insensitivity and ease of synthesis are also necessary so that the CIL can serve for the industrialization of indoor OPV cells [18]. Currently, many high-performance CIL materials have been developed, such as ZnO[19, 20], PFN-Br [21], PDINN [22], PNDIT-F3N and PNDIT-F3N-Br [23], which exhibit outstanding performance and wide utilization in the OPV field. Unfortunately, most of them still present certain drawbacks that hinder the industrialization and applications of indoor OPV cells. For instance, PFN-Br is sensitive to thickness, and PNDIT-F3N-Br is difficult to synthesize. PDINN and PNDIT-F3N contain alkalic and nucleophilic groups which can deteriorate the active layer and electrode during the operation of OPV cells [12, 14]. Thus, it is urgent to develop new CIL materials that can meet the requirements of indoor applications. Inspiringly, Xia et al. [24] reported the synthesis of diverse carbonyl materials that can exhibit prominent performance in OPV cells. Moreover, Xia and He et al. [25] reported a unique material called dicarbonyl-phenanthroline (DCP), which can be utilized as an alternative CIL for OPV cells. The DCP-based OPV cells obtain a high PCE of 18.2% and the perovskite/organic tandem cells reach an impressive PCE of 21.7%. DCP is insensitive to film thickness, and more importantly, it is a material with weak alkalinity and nucleophilicity, which is beneficial to obtain high stability of OPV cells, and this is because both ends of phenanthroline are connected by an electron-deficient carbonyl framework with large steric hindrance. Thereby, DCP exhibits great potential for the indoor applications of OPV cells. However, the research about the detailed properties and the indoor applications of DCP is still lacking.

In this work, we investigated the performance of DCP for indoor OPV cells compared with the well-known PDINN and PNDIT-F3N, and explored the application of indoor OPV modules for efficient wireless power transfer. DCP possesses suitable energy level, favorable transmittance and high conductivity. Moreover, we demonstrated a slightly decreased depletion region width of DCP through Mott-Schottky analysis, which is beneficial for charge extraction and therefore improves the photovoltaic performance of indoor OPV cells. The OPV cells also maintained superior stability under indoor lighting benefitting from the absence of strong

alkalinity of DCP, which realizes a T80 lifetime (the time for reaching 80% of the initial PCE value) of 32000 hours. Furthermore, DCP exhibits excellent adaptability for coating process due to its thickness insensitivity. Thus, we fabricated an OPV module with an effective area of  $1.5 \text{ cm}^2$  by blade coating and integrated this module with a wireless device. The module achieves a high maximum output voltage ( $V_{\text{max}}$ ) of 4.00 V, an impressive PCE of 30.6% and a maximum output power ( $P_{\text{max}}$ ) of  $142 \text{ }\mu\text{W}$  at 1000 lux. This is the state-of-the-art result for indoor OPV module. It is assumed that the OPV module works 12 hours one day at 500 lux. The energy provided by one OPV module can refresh the electronic paper 13 times for the wireless device. These results demonstrate the prominent potential of DCP-based OPV cells for indoor applications and provide an application pathway for wireless devices through indoor OPV modules.

## 2. Results and Discussions

Among the commonly used CIL materials, PDINN and PNDIT-F3N with high performance and thickness insensitivity are widely used for the fabrication of OPV cells [26, 27]. Therefore, we selected PDINN and PNDIT-F3N as comparison and comprehensively investigated the properties of DCP, PDINN and PNDIT-F3N for indoor OPV cells. The chemical structures of DCP, PDINN and PNDIT-F3N are shown in **Figure 1a**. We measured the transmission and absorption spectra of DCP, PDINN and PNDIT-F3N. The corresponding films are deposited through the optimized processes that are used during the fabrications of OPV cells, and the film thicknesses are 8, 12 and 6 nm for DPC, PDINN and PNDIT-F3N, respectively. All of them show high transmittance over 90% in the range of 400-800 nm (**Figure 1b**), which is beneficial to reduce the light absorption of CIL. In consistent with the ultraviolet-visible absorption spectra (**Figure S1a**), DCP presents a maximum absorption peak at 560 nm, while the maximum absorption peaks of PDINN and PNDIT-F3N are located at 500 and 390 nm, respectively. Meanwhile, DCP exhibits a medium absorbance at the optimal film thickness compared with PDINN and PNDIT-F3N.

Ultraviolet photoelectron spectroscopy (UPS) was carried out to measure the work function (WF) of DCP, PDINN and PNDIT-F3N (**Figure 1c**). The secondary electron cut-off edges of DCP, PDINN and PNDIT-F3N are 18.2, 18.4 and 18.7 eV, respectively. As shown in **Figure 1c** (left), DCP exhibits a higher WF of 3.87 eV than PDINN (3.63 eV) and PNDIT-F3N (3.84 eV). The highest occupied molecular orbit (HOMO) and lowest unoccupied molecular orbit (LUMO) energy levels are further measured by cyclic voltammetry measurement (**Figure S1b**). DCP, PDINN and PNDIT-F3N show similar LUMO levels of -4.06, -4.09 and -4.08 eV, respectively. This indicates that the difference of LUMO levels between active layer and DCP is favorable for charge extraction at the interface. Moreover, DCP has a deeper HOMO level of -6.17 eV in comparison with PDINN (-5.98 eV) and PNDIT-F3N (-5.55 eV), which can effectively block the hole transfer. These results suggest that DCP has suitable energy levels to act as a high-performance CIL material. The energy levels of the materials are summarized in **Figure 1d**.

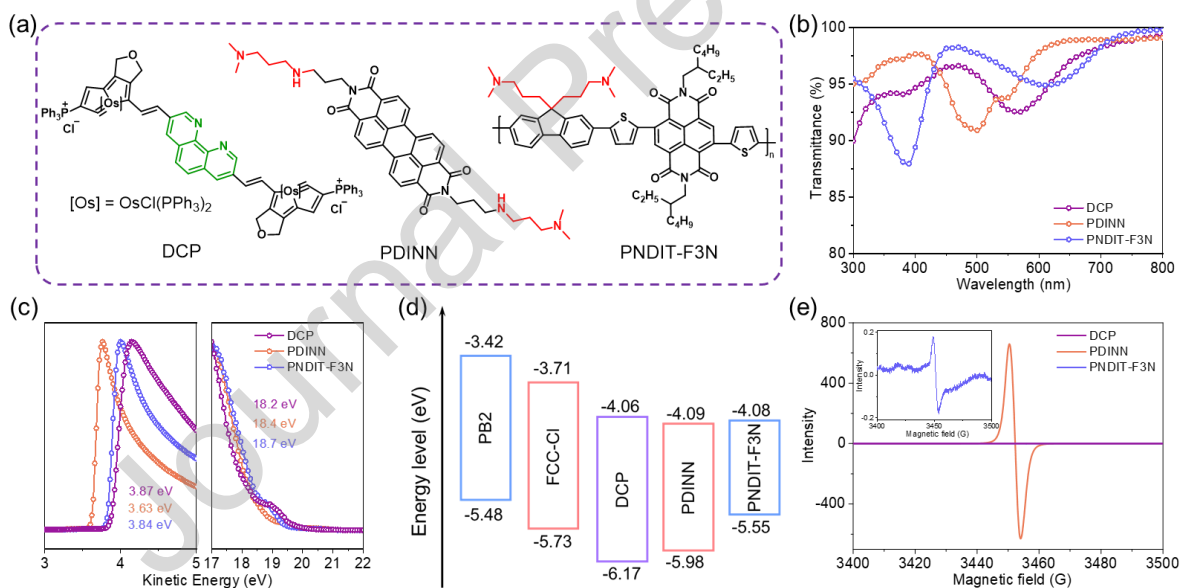


**Figure 1.** (a) The chemical structures, (b) the transmission spectra and (c) UPS spectra of DCP, PDINN and PNDIT-F3N. (d) The energy levels of the materials used in this work. (e) ESR spectra of DCP, PDINN and PNDIT-F3N.

Furthermore, electron spin resonance (ESR) spectroscopy was performed to compare the self-doping state of DCP, PDINN and PNDIT-F3N. As depicted in **Figure 1e**, PDINN exhibits the strongest ESR signal of nitrogen vacancy, suggesting the strong self-doping effect of PDINN, while PNDIT-F3N shows a weak doping effect implied by a lower ESR signal. The

results are consistent with the previous literature [22, 23]. Differing from PDINN and PNDIT-F3N, the ESR signal of nitrogen vacancy is negligible in DCP, which demonstrates that there is no self-doping effect of the phenanthroline unit in DCP. The thickness insensitivity of DCP can be attributed to the high conductivity of DCP due to the existence of Os atoms. Thus, the bulk conductivities of DCP, PDINN and PNDIT-F3N were further estimated based on the current-voltage ( $I$ - $V$ ) curves of the corresponding devices. DCP presents a comparable conductivity of  $7.59 \times 10^{-4} \text{ S m}^{-1}$  with  $7.51 \times 10^{-4} \text{ S m}^{-1}$  of PDINN, which is obviously higher than that of PNDIT-F3N ( $5.78 \times 10^{-4} \text{ S m}^{-1}$ ) (**Figure 2a**). The high conductivity of DCP is conducive to decreasing the charge accumulation and suppressing the charge recombination, thereby contributing to enhanced performance of the OPV cells.

The depletion region widths at the bulk-heterojunction (BHJ)/CIL interface and the CIL/electrode interface are the critical parameters which significantly affect the charge extraction and transport. Therefore, we conducted a detailed investigation on the depletion region widths at CIL/Ag and BHJ/CIL interface [28]. As displayed in **Figure 2b**, the depletion region width at the CIL/Ag and BHJ/CIL interface can be expressed as  $\lambda_a$  and  $\lambda_b$ , respectively. The  $\lambda_a$  can be calculated using the equation 1:

$$\lambda_a = \left( \frac{2\varepsilon_0\varepsilon_r V_{bi}}{qN_d} \right)^{\frac{1}{2}} \quad (1)$$

where  $\varepsilon_0$  is the permittivity of vacuum,  $\varepsilon_r$  is the relative dielectric constant,  $q$  is the elementary charge,  $V_{bi}$  is the absolute value of the  $E_F/q$  difference between CIL and Ag,  $N_d$  is the doping density of the CIL. The  $\lambda_b$  can be calculated using the equation 2:

$$\lambda_b = \left[ \frac{2\varepsilon_0\varepsilon_r V_{bi}}{q} \left( \frac{N_d^{BHJ}}{N_d} \right) \left( \frac{1}{N_d^{BHJ} + N_d} \right) \right]^{\frac{1}{2}} \quad (2)$$

where  $V_{bi}$  is the absolute value of the  $E_F/q$  difference between CIL and BHJ,  $N_d^{BHJ}$  is the doping density of the BHJ. Herein, PB2:FCC-Cl [29, 30] is selected as the BHJ to fabricate the devices and their chemical structures are shown in **Figure S2**.

According to the frequency-dependent capacitance characteristic, the  $\varepsilon_s$  can be calculated from the capacitance at 10 kHz, which are 4.16, 4.10 and 2.18 for DCP, PDINN and PNDIT-

F3N, respectively (**Figure S3a** and **equation S1**). In addition, the  $\epsilon_r$  of PB2:FCC-Cl is calculated to be 2.35 based on the same method (**Figure S3b**). Then, the doping density of DCP, PDINN, PNDIT-F3N and PB2:FCC-Cl are further determined based on the Mott-Schottky plots (**equation S2**). The doping densities of DCP, PDINN and PNDIT-F3N are  $8.46 \times 10^{17}$ ,  $8.70 \times 10^{17}$  and  $2.44 \times 10^{17} \text{ cm}^{-3}$ , respectively (**Figure 2c** and **Figure S4**); the doping density of PB2:FCC-Cl is also calculated to be  $1.41 \times 10^{17} \text{ cm}^{-3}$  (**Figure S5**). Surprisingly, the doping density of DCP is just slightly lower than that of PDINN and obviously higher than that of PNDIT-F3N, even though DCP exhibits negligible self-doping effect in ESR measurement. We conjecture that this special property may stem from the transition metal Os of DCP. As a result, the  $\lambda_{as}$  of DCP, PDINN and PNDIT-F3N can be calculated to be 4.81, 5.58 and 15.3 nm, respectively (**Figure 2d**). Meanwhile, the  $\lambda_{bs}$  of DCP, PDINN and PNDIT-F3N are 22.5, 24.7 and 30.8 nm, respectively. Thus, the total depletion region width ( $\lambda_a + \lambda_b$ ) of DCP (27.3 nm) is slightly thinner than that of PDINN (30.3 nm), and both of them are much smaller than that of PNDIT-F3N (46.1 nm). The reduced depletion region width of DCP results from the smaller  $V_{bi}$  values in the DCP/Ag and DCP/PB2:FCC-Cl interlayers due to the matched Fermi-levels. Theoretically, the smaller depletion region width facilitates decreasing the energy barrier for charge extraction and suppressing the charge recombination at the interface, thereby further improving the photovoltaic performance [31-33]. This result demonstrates the promising performance of DCP as a CIL material and implies that the DCP-based OPV cells should have higher PCE values under indoor lighting in comparison with the PDINN- and PNDIT-F3N-based cells.

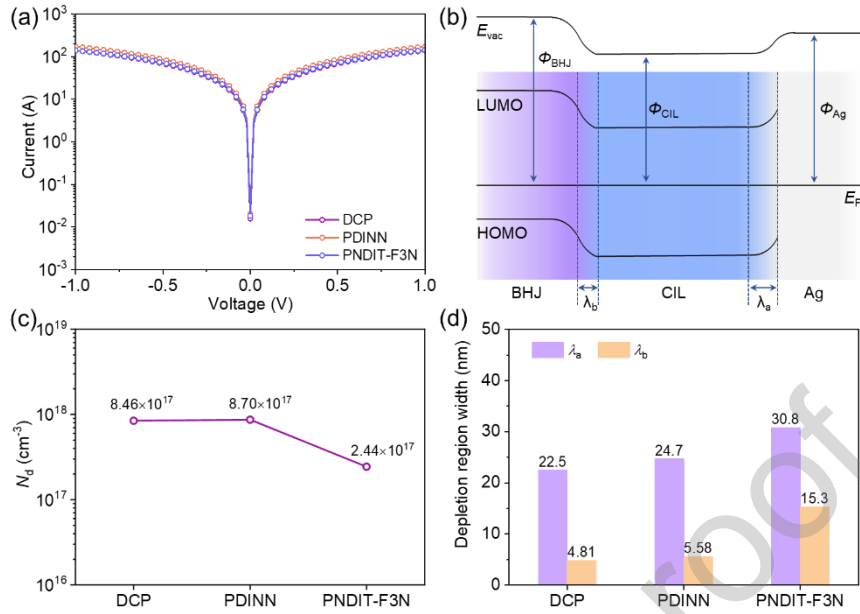


**Figure 2.** (a)  $I-V$  curves of the DCP-, PDINN- and PNDIT-F3N-based devices with the structure of ITO/CIL/Ag. (b) The schematic diagram of depletion region in BHJ/CIL/Ag interface. (c) The  $N_d$  values of DCP, PDINN and PNDIT-F3N. (d) The depletion region width of CIL/Ag ( $\lambda_a$ ) and PB2:FCC-CI/CIL ( $\lambda_b$ ) interface.

To evaluate the performance of DCP, PDINN and PNDIT-F3N, we fabricated the corresponding OPV cells and first measured the photovoltaic performance under AM 1.5G. The current density-voltage ( $J-V$ ) curves of the OPV cells are shown in **Figure 3a**. The OPV cells based on DCP and PDINN obtain similar photovoltaic performance with the same  $V_{OC}$ s of 1.08 V,  $J_{SC}$ s of 17.3 and 17.4 mA cm $^{-2}$ , FF of 77.0% and 76.9%, respectively. Thus, both of them reach a prominent PCE of 14.4%. In addition, their performances are significantly higher than that of PNDIT-F3N-based cells ( $V_{OC}$  of 1.03 V,  $J_{SC}$  of 17.0 mA cm $^{-2}$ , FF of 73.0% and PCE of 12.8%). The improvement of  $V_{OC}$  and FF in DCP-based cells can be attributed to the smaller depletion region width than PNDIT-F3N, which facilitates charge extraction and suppresses charge recombination. The device performance of OPV cells at various DCP thicknesses was further determined (**Table S1**). DCP-based cells exhibit high PCEs of over 14% at different DCP thicknesses, demonstrating satisfactory thickness insensitivity and feasibility for coating process. The external quantum efficiency (EQE) curves are depicted in **Figure 3b**. The integrated current densities ( $J_{calS}$ ) of the OPV cells based on DCP, PDINN and PNDIT-F3N are

17.1, 16.9 and 16.8 mA cm<sup>-2</sup>, respectively, which are consistent with the  $J_{SCs}$ . The related results are summarized in **Table 1**. The improvement of EQE observed in the DCP-based cell should be attributed to the charge transfer occurring between PB2 and DCP. Thus, we fabricated a double-layer device with the structure of ITO/PEDOT:PSS/PB2/DCP/Al. The device gives a  $V_{OC}$  of 1.05 V and a  $J_{SC}$  of 0.105 mA cm<sup>-2</sup>, indicating that charge transfer and dissociation can occur at the interface of PB2/DCP (**Figure S6**).

**Table 1.** The detailed photovoltaic parameters of the OPV cells based on DCP, PDINN and PNDIT-F3N under AM 1.5G.

CIL	$V_{OC}$ (V)	$J_{SC}$ (mA cm <sup>-2</sup> )	$J_{cal}$ (mA cm <sup>-2</sup> ) <sup>a</sup>	FF (%)	PCE (%) <sup>b</sup>
DCP	1.08	17.3	17.1	77.0	14.4 (14.1±0.2)
PDINN	1.08	17.4	16.9	76.9	14.4 (14.1±0.2)
PNDIT-F3N	1.03	17.0	16.8	73.0	12.8 (12.5±0.2)

<sup>a</sup>The  $J_{cal}$ s are integrated from the EQE curves.

<sup>b</sup>The average PCEs with standard deviations in parentheses are obtained from 6 individual cells.

Furthermore, we measured the indoor performance of OPV cells based on DCP, PDINN and PNDIT-F3N to evaluate the performance of DCP under weak illumination. As shown in **Figure 3c**, a 2700 K LED light is applied to provide the indoor lighting of 1000, 500 and 200 lux. The corresponding  $J$ - $V$  curves are shown in **Figure 3d** and **Figure S7**. The OPV cells based on PNDIT-F3N, PDINN and DCP exhibit increasing  $V_{OCs}$  of 0.903, 0.920 and 0.926 V at 1000 lux, respectively. This characteristic results from enhanced influences of depletion region width due to decreased carrier density under weak illumination, resulting in increased charge recombination at interlayer. Thus, the DCP-based cells have lower voltage losses than that of PDINN and PNDIT-F3N under indoor lighting benefiting from the smaller depletion region width, which demonstrates the superiority of DCP for indoor OPV cells. Moreover, DCP-based cells obtain a comparable  $J_{SC}$  of 126  $\mu$ A cm<sup>-2</sup> and improved FF of 80.7% in comparison with that of PDINN and PNDIT-F3N at 1000 lux. Thus, the OPV cells based on DCP achieve a remarkable PCE of 30.4%, which is one of the state-of-the-art results for indoor OPV cells. In contrast, the PDINN-based cells obtain a PCE of 29.1%, while the PNDIT-F3N-based cells give

a lower PCE of 28.4% due to the restricted  $V_{OC}$  and FF. As the illuminance decreases, the  $V_{OC}$  and FF values of three OPV cells gradually decrease, resulting in reduced PCEs under very weak illumination. Nonetheless, the DCP-based cells still reach a satisfactory PCE of 28.8% and 26.3% at 500 and 200 lux, which also exceeds the performance of PDINN- and PNDIT-F3N-based cells. The detailed photovoltaic parameters are summarized in **Table 2**. The increasing photovoltaic performance of DCP-based cells indicates the outstanding performance of DCP for indoor photovoltaics.

**Table 2.** The detailed photovoltaic parameters of the OPV cells based on DCP, PDINN and PNDIT-F3N under indoor lighting.

CIL	Illuminance (lux)	$P_{in}$ ( $\mu\text{W cm}^{-2}$ )	$V_{OC}$ (V)	$J_{SC}$ ( $\mu\text{A cm}^{-2}$ )	$J_{cal}$ ( $\mu\text{A cm}^{-2}$ ) <sup>a</sup>	FF (%)	$P_{out}$ ( $\mu\text{W cm}^{-2}$ )	PCE (%) <sup>b</sup>
DCP	1000	310	0.926	126	120	80.7	94.2	30.4 (29.8±0.4)
	500	154	0.896	62.6	59.6	79.0	44.3	28.8 (28.6±0.2)
	200	60.7	0.861	24.5	23.7	75.8	16.0	26.3 (26.2±0.2)
PDINN	1000	310	0.920	123	118	79.8	90.3	29.1 (28.8±0.4)
	500	154	0.896	61.2	58.8	79.0	43.3	28.1 (27.8±0.4)
	200	60.7	0.860	24.2	23.3	74.1	15.4	25.4 (25.2±0.2)
PNDIT-F3N	1000	310	0.903	124	118	78.5	87.9	28.4 (28.0±0.4)
	500	154	0.874	61.2	58.7	78.0	41.7	27.1 (27.0±0.4)
	200	60.7	0.841	24.4	23.3	73.9	15.2	25.0 (24.6±0.3)

<sup>a</sup>The  $J_{cal}$ s are integrated from the EQE curves based on the emission spectra of 2700 K LED light.

<sup>b</sup>The average PCEs with standard deviations in parentheses are obtained from 6 individual cells.

Since DCP-based OPV cells exhibit improved  $V_{OC}$  and FF under indoor lighting, the charge transport and recombination are further investigated. Electrochemical impedance spectroscopy was performed to measure the series resistance ( $R_{series}$ ). The Nyquist plots are fitted using the equivalent circuit model in **Figure 3e**. The DCP-, PDINN- and PNDIT-F3N-based OPV cells have approximate  $R_{series}$  values of 1.72, 1.65, 1.60  $\Omega \text{ cm}^2$ , respectively. Then, the fast carrier mobility is determined by photo-induced charge carrier extraction by linear increasing voltage (photo-CELIV). According to **Figure S8**, the fast carrier mobilities are calculated to be  $2.57 \times 10^{-4}$

$4$ ,  $2.63 \times 10^{-4}$  and  $2.69 \times 10^{-4} \text{ cm}^2 \text{ V}^{-1} \text{ s}^{-1}$  for the OPV cells based on DCP, PDINN and PNDIT-F3N, respectively. These results suggest that DCP exhibits comparable charge transport ability with PDINN and PNDIT-F3N. The charge transport ability is not the dominated factor for improved photovoltaic performance of DCP-based cells.

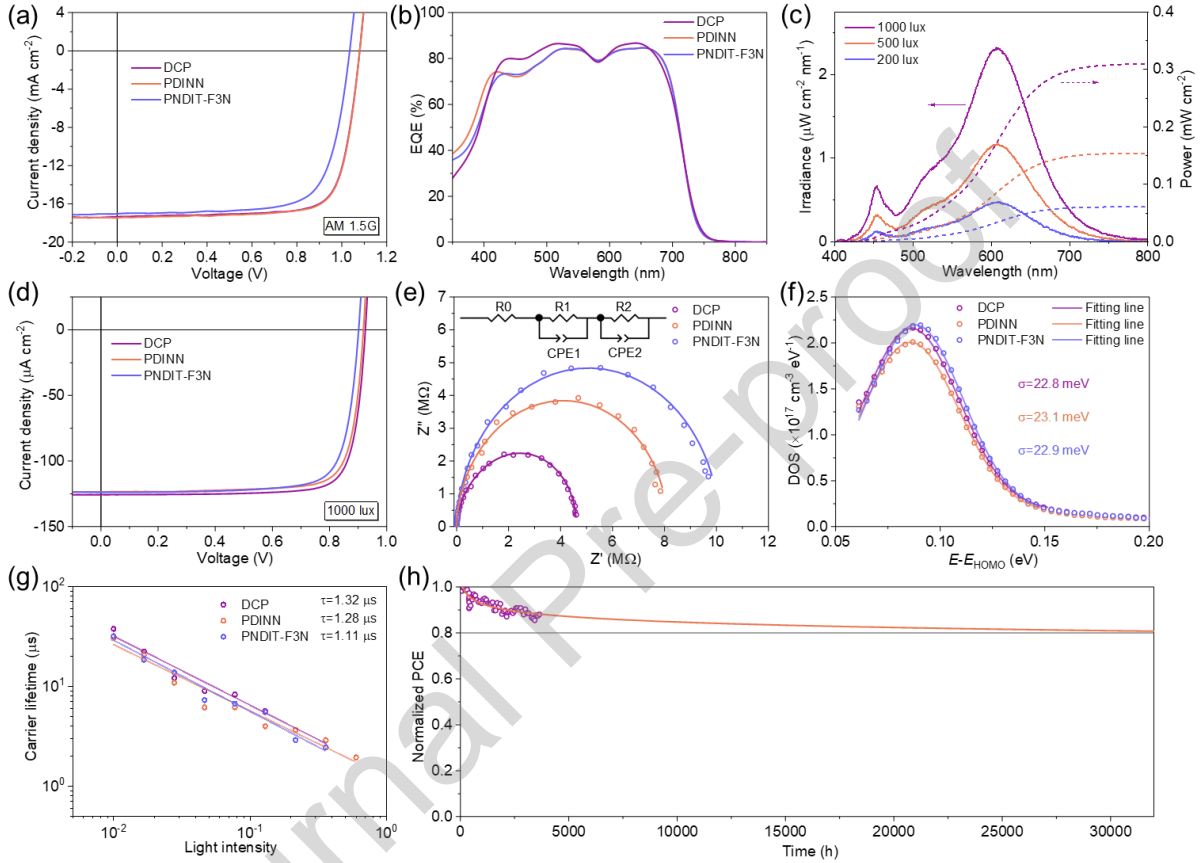


**Figure 3.** (a) The  $J$ - $V$  curves of the OPV cells under AM 1.5G. (b) The EQE curves of the optimized OPV cells. (c) The emission spectra and the power density of 1000, 500 and 200 lux LED light (2700 K). (d) The  $J$ - $V$  curves of the OPV cells at 1000 lux. (e) The EIS spectra, (f) DOS distribution and (g) TPV measurement of the corresponding cells. (h) The device stability of the DPC-based cell at 1000 lux.

The density of state (DOS) distribution was analyzed by capacitance spectroscopy. The OPV cell based on DCP exhibits larger  $\varepsilon_t$  than that of PDINN and PNDIT-F3N, which benefits the charge extraction (**Figure S9a**). Combined with Mott-Schottky characterization (**Figure S9b**), the DOS distribution of the corresponding OPV cells can be plotted in **Figure 3f**. Then, the energy disorder parameter ( $\sigma$ ) can be extracted through the equation 3 [34]:

$$N_t(E) = \frac{N_t}{\sqrt{2\pi}\sigma} \exp\left[-\frac{(E_t - E)^2}{2\sigma^2}\right] \quad (3)$$

where  $N_t$  is the total trap density and  $E_t$  is the center of DOS. By Gaussian fitting, the  $\sigma$  values of DCP-, PDINN- and PNDIT-F3N-based cells are calculated to be 22.8, 23.1 and 22.9 meV, respectively. It is suggested that the DCP-based cells can obtain a relatively small DOS distribution in favor of high performance, which is beneficial to suppressing the voltage losses under indoor lighting [35, 36]. Transient photo-voltage (TPV) measurement is performed to analyze the charge recombination. As shown in **Figure 3g**, the charge carrier lifetime of DCP-based OPV cell is 1.32  $\mu$ s, which is higher than that of PDINN (1.28  $\mu$ s) and PNDIT-F3N (1.11  $\mu$ s), demonstrating efficient charge extraction and decreased charge recombination. Then, the charge recombination is further discussed based on light intensity-dependent  $V_{OC}$  and  $J_{SC}$ . For the relationship between  $V_{OC}$  and light intensity ( $P_{in}$ ), the DCP-based cells exhibit a slope of  $1.28 kT q^{-1}$  (where  $k$  is Boltzmann constant,  $T$  is Kelvin temperature and  $q$  is elementary charge), which is consistent with that of PDINN ( $1.26 kT q^{-1}$ ) but smaller than that of PNDIT-F3N ( $1.32 kT q^{-1}$ ) (**Figure S10a**). This result suggests that the DCP-based cells have relatively low trap-assist recombination. In addition, the relationship between  $J_{SC}$  and  $P_{in}$  is shown in **Figure S10b**. The OPV cells based on DCP, PDINN and PNDIT-F3N obtain similar slopes of  $J_{SC}$ - $P_{in}$ , implying that bimolecular recombination is non-dominated. These results demonstrate that DCP exhibits similar performance with PDINN for OPV cells, but better than PNDIT-F3N.

We further evaluated the device stability of DCP-based OPV cells at continuous illumination of 1000 lux. After being illuminated for 3640 h, the PCE of DCP-based cell maintains 88% of the initial values (**Figure S11**). By tracking the trend of the PCE evolution, the fitting T80 lifetime is estimated to be 32000 h (**Figure 3h**), demonstrating the prominent stability of DCP-based OPV cell under indoor lighting. The prominent stability is attributed to the weak alkalinity of DCP, which is not enough to damage the active layer and electrode during the operation of devices. The absence of strongly alkaline groups also results in more stable interlayer structure and thus contributes to the long-term device stability. Therefore, these results demonstrate the promising potential of DCP for stable and efficient indoor OPV cells.

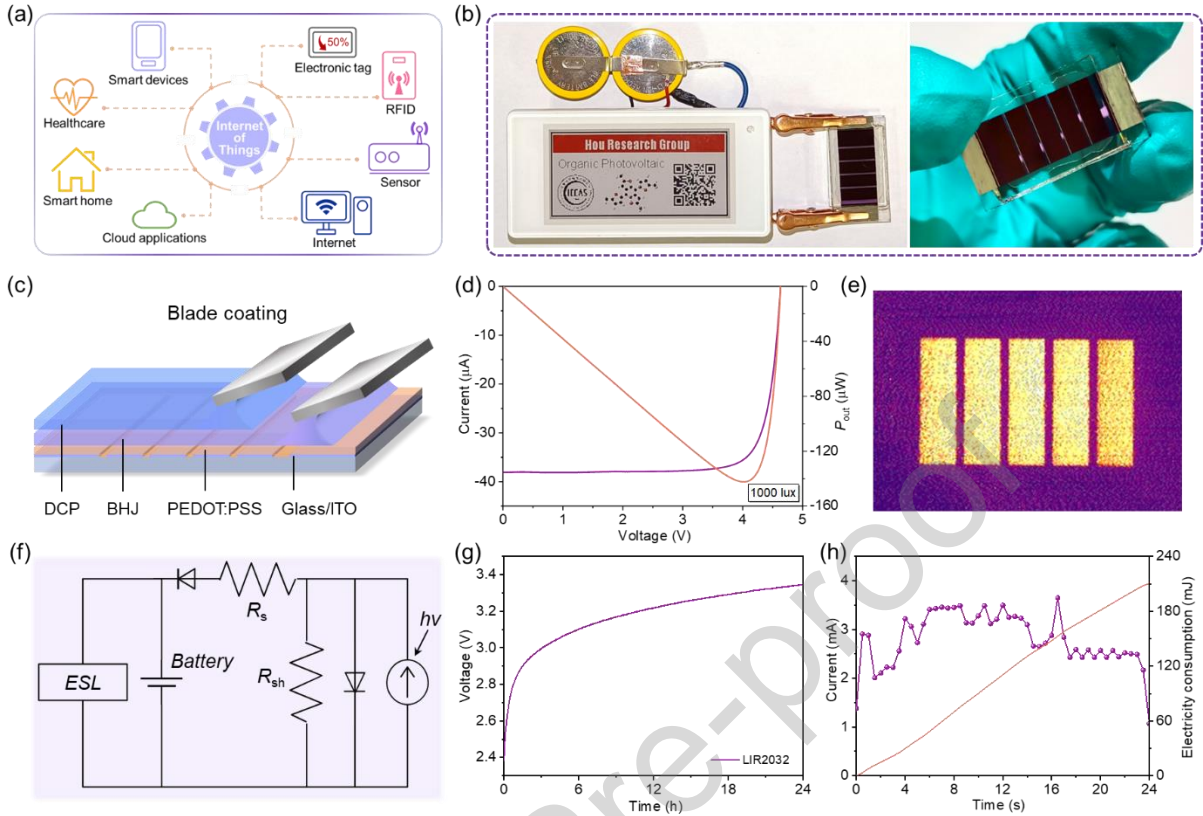


**Figure 4.** (a) The schematic of the applications for Internet of Things. (b) The photograph of the wireless devices integrating ESL, lithium cells and OPV module (left) and the photograph of DCP-based OPV module (right). (c) The schematic of the blade coating process for OPV modules. (d) The  $I$ - $V$  and  $P_{out}$  curves of the OPV module at 1000 lux. (e) The EQE mapping of the OPV module. (f) The equivalent circuit diagram of the integrated system. (g) The charging curve of lithium battery (LIR2032) through the OPV module at 1000 lux. (h) The current variation and electricity consumption of the wireless device for refreshing once.

As we all know, the indoor OPV cells exhibit unique advantages for the Internet of Things applications, such as smart devices, wireless sensors, radio-frequency identification (RFID) devices, electronic tags and etc. [37] (**Figure 4a**). Therefore, we investigated the feasibility of the integration of DCP-based OPV cell with wireless devices (**Figure 4b**). We selected a commercial electronic shelf label (ESL) that is a representative wireless device widely used in market. The ESL generally contains an electronic paper, a control module with Bluetooth and two parallel lithium batteries (CR2450). When the ESL needs to be refreshed, the Bluetooth module accepts the command and the lithium batteries supply electricity to the control module and electronic paper. Then, the electronic paper can be refreshed. Otherwise, the ESL will stay

in a state with extremely low power consumption, and the contents on electronic paper can be maintained without energy supplement. However, the lithium battery (CR2450) just provides limited electric energy, and it is time-consuming and high-cost to frequently replace the battery for numerous ESL. The integration of OPV cells with lithium battery is a promising power supply method for ESL due to the advantages of high efficiency under weak illumination, light weight and nontoxicity of OPV cells.

To realize the self-power function, the non-rechargeable lithium batteries (CR2450) are replaced with two rechargeable lithium batteries (LIR2032) in parallel, each of which can provide a voltage of 3.6 V. To reach the voltage for charging lithium battery (LIR2032), we designed an OPV module including 5 sub-cells (**Figure 4b**). The OPV module has an effective area of 1.5 cm<sup>2</sup>, which is a delicate size for ESL so that the OPV module is expected to be integrated inside the ESL. We further fabricated the OPV module by sequentially blade coating the active layer and DCP interlayer (**Figure 4c**). The thickness of DCP layer is about 26 nm. The photovoltaic performance of the module was determined under AM 1.5G and indoor lighting, respectively. The detailed parameters are shown in **Table S2**. Under AM 1.5G, the OPV module reaches a high  $V_{OC}$  of 5.35 V, a short-circuit current ( $I_{SC}$ ) of 5.07 mA and an FF of 76.9%, giving an excellent PCE of 13.9% (**Figure S12a**). At 1000 lux, the OPV module obtains a high  $V_{OC}$  of 4.63 V, an  $I_{SC}$  of 38.1  $\mu$ A and an optimal FF of 80.7%, contributing to a remarkable PCE of 30.6% (**Figure 4d**), which is a state-of-the-art performance for indoor OPV modules. Importantly, the OPV module gives a  $P_{max}$  of 142  $\mu$ W with a  $V_{max}$  of 4.00 V and a maximum current ( $I_{max}$ ) of 35.6  $\mu$ A. Even at 500 lux, a considerable  $V_{OC}$  of 4.49 V and an  $I_{SC}$  of 18.7  $\mu$ A can also be reached, corresponding to a PCE of 28.3% (**Figure S12b**). Meanwhile, a  $V_{max}$  of 3.86 V and an  $I_{max}$  of 16.9  $\mu$ A are provided to give a  $P_{max}$  of 65.2  $\mu$ W, which can still meet the requirement for charging the lithium battery (LIR2032).

Moreover, the EQE mapping of the optimal OPV module was measured. Generally, the deposition process during blade coating is difficult to control and the thickness-sensitive CIL also brings challenges for the coating process of OPV modules. According to **Figure 4e**, the OPV module exhibits a uniform film with high EQE response, which demonstrates the high

adaptability of DCP for blade coating process benefiting from its thickness insensitivity. This indicates the notable advantages of DCP for the manufacture of indoor OPV modules in favor of the industrialization.

Finally, the OPV module is connected in series with the lithium batteries by using a diode to avoid the reverse charging, and then the integration of OPV module with ESL can be realized (**Figure 4b** and **Figure S13**). The equivalent circuit diagram of the integrated system is shown in **Figure 4f**. We measured the charging process of lithium battery (LIR2032) using the indoor OPV module as energy source. The corresponding charging curve is demonstrated in **Figure 4g**, indicating feasible charging process. The capacitance variation of lithium battery in charging process is demonstrated in **Figure S14**. We further determined the electricity consumption of ESL for refreshing one time (about 24 s). The voltage is determined to be 3.09 V and the current variation during this process is shown in **Figure 4h**. The average electricity consumption for refreshing one time is calculated to be 210 mJ. We assume that the OPV module works at 500 lux indoor lighting for 12 hours one day. The energy provided by one OPV module can refresh an ESL 13 times. These results demonstrate the promising applications of the OPV modules for efficient wireless power transfer. In addition, benefitting from the high  $V_{\max}$ , the indoor OPV module can be also potentially applied for smart devices, fingerprint locks, digital peepholes, etc., showing wide application prospects.

### 3. Conclusion

In conclusion, we comprehensively investigated the performance of DCP as a CIL for indoor applications in comparison with PDINN and PNDIT-F3N. DCP exhibits a high transmittance, high conductivity and favorable energy level. Although DCP is free of self-doping effect, it presents thinner depletion region width due to the existence of transition metal Os. This contributes to suppressed charge recombination and voltage losses. As a result, the DCP-based OPV cell obtains a prominent PCE of 14.4% under AM 1.5G, and meanwhile achieves an excellent PCE of 30.4% at 1000 lux. The DCP-based cell also retains outstanding device stability with a T80 lifetime of 32000 h. The slightly enhanced photovoltaic performance of

DCP-based cells than that of PDINN demonstrates the excellent properties of DCP for indoor OPV applications. Importantly, we fabricated a DCP-based OPV module by blade coating and investigated its application for wireless power transfer. The OPV module reaches a high  $V_{OC}$  of 4.63 V and a remarkable PCE of 30.6% at 1000 lux. The electricity energy supplied by this OPV module can refresh the ESL 13 times a day. Overall, this work realizes a highly efficient indoor OPV module using DCP as the cathode interlayer and demonstrates the practical feasibility of indoor OPV module for efficient wireless power transfer.

### **Acknowledgments**

This work was supported by the National Natural Science Foundation of China (Nos. 52120105005, 22322904 and 22275195). Y.C. acknowledges the financial support from the Youth Innovation Promotion Association of the Chinese Academy of Sciences (No. 2023036). H. X. is supported by the Introduction of Major Talent Projects in Guangdong Province (No. 2019CX01C079).

### **Declaration of Competing Interest**

The authors declare that they have no known competing financial interests or personal relationships that could have appeared to influence the work reported in this paper.

## References

- [1] D. Müller, E. Jiang, P. Rivas-Lazaro, C. Baretzky, G. Loukeris, S. Bogati, S. Paetel, S.J.C. Irvine, O. Oklobia, S. Jones, D. Lamb, A. Richter, G. Siefer, D. Lackner, H. Helmers, C. Teixeira, D. Forgács, M. Freitag, D. Bradford, Z. Shen, B. Zimmermann, U. Würfel, Indoor Photovoltaics for the Internet-of-Things – A Comparison of State-of-the-Art Devices from Different Photovoltaic Technologies, *ACS App. Energy Mater.* 6 (2023) 10404-10414.
- [2] A. Panagiotopoulos, T. Maksudov, G. Kakavelakis, G. Perrakis, E.A. Alharbi, D. Kutsarov, F.H. Isikgor, S. Alfihed, K. Petridis, M. Kafesaki, S.R.P. Silva, T.D. Anthopoulos, M. Graetzel, A critical perspective for emerging ultra-thin solar cells with ultra-high power-per-weight outputs, *Appl. Phys. Rev.* 10 (2023) 041303.
- [3] Q. Wu, Y. Yu, X. Xia, Y. Gao, T. Wang, R. Sun, J. Guo, S. Wang, G. Xie, X. Lu, E. Zhou, J. Min, High-performance organic photovoltaic modules using eco-friendly solvents for various indoor application scenarios, *Joule* 6 (2022) 2138-2151.
- [4] Y. Cui, L. Hong, J. Hou, Organic Photovoltaic Cells for Indoor Applications: Opportunities and Challenges, *ACS Appl. Mater. Interfaces* 12 (2020) 38815-38828.
- [5] M. Jahandar, S. Kim, D.C. Lim, Indoor Organic Photovoltaics for Self - Sustaining IoT Devices: Progress, Challenges and Practicalization, *ChemSusChem* 14 (2021) 3449-3474.
- [6] Y. Cui, Y. Xu, J. Hou, High efficiency and more functions bring a bright future for organic photovoltaic cells, *Sci. Bull.* 67 (2022) 1300-1303.
- [7] S. Park, H. Ahn, J.-y. Kim, J.B. Park, J. Kim, S.H. Im, H.J. Son, High-Performance and Stable Nonfullerene Acceptor-Based Organic Solar Cells for Indoor to Outdoor Light, *ACS Energy Lett.* 5 (2019) 170-179.
- [8] T. Zhang, C. An, Y. Xu, P. Bi, Z. Chen, J. Wang, N. Yang, Y. Yang, B. Xu, H. Yao, X. Hao, S. Zhang, J. Hou, A Medium-Bandgap Nonfullerene Acceptor Enabling Organic Photovoltaic Cells with 30% Efficiency under Indoor Artificial Light, *Adv. Mater.* 34 (2022) e2207009.
- [9] P. Bi, C. An, T. Zhang, Z. Chen, Y. Xu, Y. Cui, J. Wang, J. Li, Y. Wang, J. Ren, X. Hao, S. Zhang, J. Hou, Achieving 31% efficiency in organic photovoltaic cells under indoor light using a low energetic disorder polymer donor, *J. Mater. Chem. A* 11 (2023) 983-991.
- [10] W. Wang, Y. Cui, T. Zhang, P. Bi, J. Wang, S. Yang, J. Wang, S. Zhang, J. Hou, High-performance organic photovoltaic cells under indoor lighting enabled by suppressing energetic disorders, *Joule* 7 (2023) 1067-1079.
- [11] C. Lee, J.H. Lee, H.H. Lee, M. Nam, D.H. Ko, Over 30% Efficient Indoor Organic Photovoltaics Enabled by Morphological Modification Using Two Compatible Non - Fullerene Acceptors, *Adv. Energy Mater.* 12 (2022) 2200275.
- [12] Z. Yin, S. Mei, P. Gu, H.Q. Wang, W. Song, Efficient organic solar cells with superior stability based on PM6:BTP-eC9 blend and AZO/Al cathode, *iScience* 24 (2021) 103027.
- [13] H. Liu, Y. Li, S. Xu, Y. Zhou, Z.a. Li, Emerging Chemistry in Enhancing the Chemical and Photochemical Stabilities of Fused - Ring Electron Acceptors in Organic Solar Cells, *Adv. Funct. Mater.* 31 (2021) 2106735.

- [14] T.L.H. Mai, S. Jeong, S. Kim, S. Jung, J. Oh, Z. Sun, J. Park, S. Lee, W. Kim, C. Yang, Over 18.2% - Efficiency Organic Solar Cells with Exceptional Device Stability Enabled by Bay - Area Benzamide - Functionalized Perylene Diimide Interlayer, *Adv. Funct. Mater.* 33 (2023) 2303386.
- [15] Z. Chen, T. Wang, Z. Wen, P. Lu, W. Qin, H. Yin, X.-T. Hao, Trap State Induced Recombination Effects on Indoor Organic Photovoltaic Cells, *ACS Energy Lett.* 6 (2021) 3203-3211.
- [16] Y. Cui, Y. Wang, J. Bergqvist, H. Yao, Y. Xu, B. Gao, C. Yang, S. Zhang, O. Inganäs, F. Gao, J. Hou, Wide-gap non-fullerene acceptor enabling high-performance organic photovoltaic cells for indoor applications, *Nat. Energy* 4 (2019) 768-775.
- [17] J. Yao, T. Kirchartz, M.S. Vezié, M.A. Faist, W. Gong, Z. He, H. Wu, J. Troughton, T. Watson, D. Bryant, J. Nelson, Quantifying Losses in Open-Circuit Voltage in Solution-Processable Solar Cells, *Phys. Rev. Applied* 4 (2015) 014020.
- [18] Y. Yu, Y. Cui, T. Zhang, Z. Chen, Y. Xiao, W. Wang, Y. Yang, N. Yang, J. Hou, An Interfacial Material with Low Trap Density Enables Efficient Organic Photovoltaic Cells for Multi - Scene Applications, *Adv. Funct. Mater.* 33 (2023) 2306095.
- [19] Y.-J. Huang, H.-C. Chen, H.-K. Lin, K.-H. Wei, Doping ZnO Electron Transport Layers with MoS<sub>2</sub> Nanosheets Enhances the Efficiency of Polymer Solar Cells, *ACS Appl. Mater. Interfaces* 10 (2018) 20196-20204.
- [20] H.-C. Chen, S.-W. Lin, J.-M. Jiang, Y.-W. Su, K.-H. Wei, Solution-Processed Zinc Oxide/Polyethylenimine Nanocomposites as Tunable Electron Transport Layers for Highly Efficient Bulk Heterojunction Polymer Solar Cells, *ACS Appl. Mater. Interfaces* 7 (2015) 6273-6281.
- [21] F. Huang, H. Wu, D. Wang, W. Yang, Y. Cao, Novel Electroluminescent Conjugated Polyelectrolytes Based on Polyfluorene, *Chem. Mater.* 16 (2004) 708-716.
- [22] J. Yao, B. Qiu, Z.G. Zhang, L. Xue, R. Wang, C. Zhang, S. Chen, Q. Zhou, C. Sun, C. Yang, M. Xiao, L. Meng, Y. Li, Cathode engineering with perylene-diimide interlayer enabling over 17% efficiency single-junction organic solar cells, *Nat. Commun.* 11 (2020) 2726.
- [23] Z. Wu, C. Sun, S. Dong, X.F. Jiang, S. Wu, H. Wu, H.L. Yip, F. Huang, Y. Cao, n-Type Water/Alcohol-Soluble Naphthalene Diimide-Based Conjugated Polymers for High-Performance Polymer Solar Cells, *J. Am. Chem. Soc.* 138 (2016) 2004-2013.
- [24] S. Chen, L. Feng, L. Peng, X. Gao, Y. Zhu, L. Yang, D. Chen, K. Zhang, X. Guo, F. Huang, H. Xia, Synthesis and Optoelectronic Applications of d  $\pi$  - p  $\pi$  Conjugated Polymers with a Di - metallaaromatic Acceptor, *Angew. Chem.-Int. Edit.* 62 (2023) e202305489.
- [25] X. Lai, S. Chen, X. Gu, H. Lai, Y. Wang, Y. Zhu, H. Wang, J. Qu, A.K.K. Kyaw, H. Xia, F. He, Phenanthroline-carbolong interface suppress chemical interactions with active layer enabling long-time stable organic solar cells, *Nat. Commun.* 14 (2023) 3571.
- [26] T. Chen, S. Li, Y. Li, Z. Chen, H. Wu, Y. Lin, Y. Gao, M. Wang, G. Ding, J. Min, Z. Ma, H. Zhu, L. Zuo, H. Chen, Compromising Charge Generation and Recombination of Organic Photovoltaics with Mixed Diluent Strategy for Certified 19.4% Efficiency, *Adv. Mater.* 35 (2023) 2300400.
- [27] L. Zhu, M. Zhang, J. Xu, C. Li, J. Yan, G. Zhou, W. Zhong, T. Hao, J. Song, X. Xue, Z. Zhou, R. Zeng, H. Zhu, C.C. Chen, R.C.I. MacKenzie, Y. Zou, J. Nelson, Y. Zhang, Y. Sun, F.

- Liu, Single-junction organic solar cells with over 19% efficiency enabled by a refined double-fibril network morphology, *Nat. Mater.* 21 (2022) 656-663.
- [28] Y. Yang, B. Xu, J. Hou, Reducing Depletion Region Width at Electrode Interface via a Hole - transport Layer for Over 18% Efficiency in Organic Solar Cells, *Small* 20 (2023) 2306668.
- [29] T. Zhang, C. An, Y. Cui, J. Zhang, P. Bi, C. Yang, S. Zhang, J. Hou, A Universal Nonhalogenated Polymer Donor for High-Performance Organic Photovoltaic Cells, *Adv. Mater.* 34 (2022) e2105803.
- [30] F. Bai, J. Zhang, A. Zeng, H. Zhao, K. Duan, H. Yu, K. Cheng, G. Chai, Y. Chen, J. Liang, W. Ma, H. Yan, A highly crystalline non-fullerene acceptor enabling efficient indoor organic photovoltaics with high EQE and fill factor, *Joule* 5 (2021) 1231-1245.
- [31] G.D. Sharma, D. Saxena, M.S. Roy, Dark, photoelectrical properties and impedance analysis of organic semiconductor based donor/acceptor device, *Thin Solid Films* 467 (2004) 220-226.
- [32] Z. Zheng, J. Wang, P. Bi, J. Ren, Y. Wang, Y. Yang, X. Liu, S. Zhang, J. Hou, Tandem Organic Solar Cell with 20.2% Efficiency, *Joule* 6 (2021) 171-184.
- [33] Y. Yang, J. Wang, Y. Xiao, B. Xu, J. Hou, Understanding the Interfacial Energy Structure and Electron Extraction Process in Inverted Organic Solar Cells with Phosphine-Doped Cathode Interlayers, *Chin. J. Chem.* 42 (2024) 1347-1354.
- [34] S. Khelifi, K. Decock, J. Lauwaert, H. Vrielinck, D. Spoltore, F. Piersimoni, J. Manca, A. Belghachi, M. Burgelman, Investigation of defects by admittance spectroscopy measurements in poly (3-hexylthiophene):(6,6)-phenyl C61-butyric acid methyl ester organic solar cells degraded under air exposure, *J. Appl. Phys.* 110 (2011) 094509.
- [35] P. Bi, J. Ren, S. Zhang, T. Zhang, Y. Xu, Y. Cui, J. Qin, J. Hou, Suppressing Energetic Disorder Enables Efficient Indoor Organic Photovoltaic Cells With a PTV Derivative, *Front Chem* 9 (2021) 684241.
- [36] S. Leng, T. Hao, G. Zhou, L. Zhu, W. Zhong, Y. Yang, M. Zhang, J. Xu, J. Zhan, Z. Zhou, J. Chen, S. Lu, Z. Tang, Z. Shi, H. Zhu, Y. Zhang, F. Liu, Correlating Electronic Structure and Device Physics with Mixing Region Morphology in High - Efficiency Organic Solar Cells, *Adv. Sci.* 9 (2022) 2104613.
- [37] W. Kim, K. Cho, J.H. Lee, D.H. Ko, S. Jung, An Indoor Light - Powered Sensor System Integrated with Organic Photovoltaics, *Adv. Mater. Technol.* 8 (2023) 2202040.



**Wenxuan Wang** received his B.S. in chemistry at Nankai University in 2020. Currently, he is a Ph.D. student of Prof. Jianhui Hou at the State Key Laboratory of Polymer Physics and Chemistry, Institute of Chemistry, Chinese Academy of Sciences (ICCAS), University of Chinese Academy of Sciences. His research interests mainly focus on organic photovoltaic cells and organic photovoltaic materials.



**Yong Cui** received his Ph.D. degree from University of Chinese Academy of Sciences in 2019 under the supervision of Prof. Jianhui Hou. He is currently an associate professor at Institute of Chemistry, Chinese Academy of Sciences (ICCAS). His research focuses on the study of materials and device engineering toward high-performance organic photovoltaic cells for versatile applications.



**Yue Yu** received his BSc degree in department of polymer science and engineering from Sichuan University. Now he is a Ph.D. student under the supervision of Prof. Jianhui Hou at State Key Laboratory of Polymer Physics and Chemistry, Institute of Chemistry, University of Chinese Academy of Sciences, China. His main research interest is the design and synthesis of interlayer materials for high-efficiency and stable organic photovoltaic cells.



**Jianqiu Wang** received his PhD degree from Soochow University in 2022. He currently is a postdoctoral researcher in Prof. Jianhui Hou's group at Institute of Chemistry, Chinese Academy of Sciences (ICCAS). His current research interests are large-area and tandem organic solar cells.



**Chaoyi Wang** received her B.S. at Hebei University in 2021. Currently, she is a master student under the supervision of associate professor Shaoqing Zhang at school of chemistry and biological engineering, University of Science and Technology Beijing (USTB). Her research interests mainly focus on organic photovoltaic cells and polymer donor materials.



**Hao Hou** received her bachelor's degree from Beijing University of Technology. She currently is a master student in Prof. Qian Kang's group at Beijing University of Technology (BJUT). Her current research interests are interfacial layer material of organic solar cells.



**Qian Kang** received her PhD degree from the Institute of Chemistry, Chinese Academy of Sciences (ICCAS), University of Chinese Academy of Sciences under the supervision of Prof. Jianhui Hou. She currently is a

professor in Beijing University of Technology (BJUT). Her current research interests are photovoltaic devices and interfacial materials.



**Hui Wang** received a bachelor's degree in the China University of Geosciences (Wuhan) in 2022. She is currently studying as a master's degree candidate in the Department of Chemistry at the Southern University of Science and Technology under the supervision of Prof. Haiping Xia. Her research is focusing on organometallics and conjugated polymers.



**Shiyang Chen** is currently a Research Assistant Professor in the Shenzhen Grubbs Institute at the Southern University of Science and Technology. He received his Ph.D. degree in Chemistry from Xiamen University in 2021, advised by Prof. Haiping Xia. After that, he joined the Southern University of Science and Technology as a postdoc. His current research is mainly focused on the rational design and development of main-chain metals-containing conjugated polymers.



**Shaoqing Zhang** received her PhD degree in Organic Chemistry from University of Science and Technology Beijing (USTB) in 2017. She currently is an associate professor at school of chemistry and biological engineering in USTB, and her research focuses on molecular design, synthesis, and the application of highly-efficient organic photovoltaic materials.



**Haiping Xia** is a Chair Professor in Department of Chemistry at the Southern University of Science and Technology. He obtained his Ph.D. in Chemistry in 2002 from Xiamen University, where he was promoted as a Full Professor in 1999. In 2018, he moved to Southern University of Science and Technology as a Chair Professor, and has been appointed as the Executive Dean of Shenzhen Grubbs Institute since 2019. His work encompasses the synthesis, reactivities, and applications of metallaaromatics; especially the chemistry of metallapentalynes and metallapentalenes, which was also named as “Carbolong Chemistry”, was developed by him.



**Jianhui Hou** received his PhD degree in Physical Chemistry from ICCAS in 2006 (Adviser: Prof. Yongfang Li). Then he worked as a postdoctoral researcher at Prof. Yang Yang's group in University of California, Los Angeles (UCLA) from 2006 to 2008 and then as Director of Research of Solarmer Energy Inc. from 2008 to 2010. After that, he became a Full Professor at ICCAS in 2010 and an Adjunct Professor at USTB in 2012. His present research focuses on design, synthesis, and application of organic/polymer photovoltaic materials.

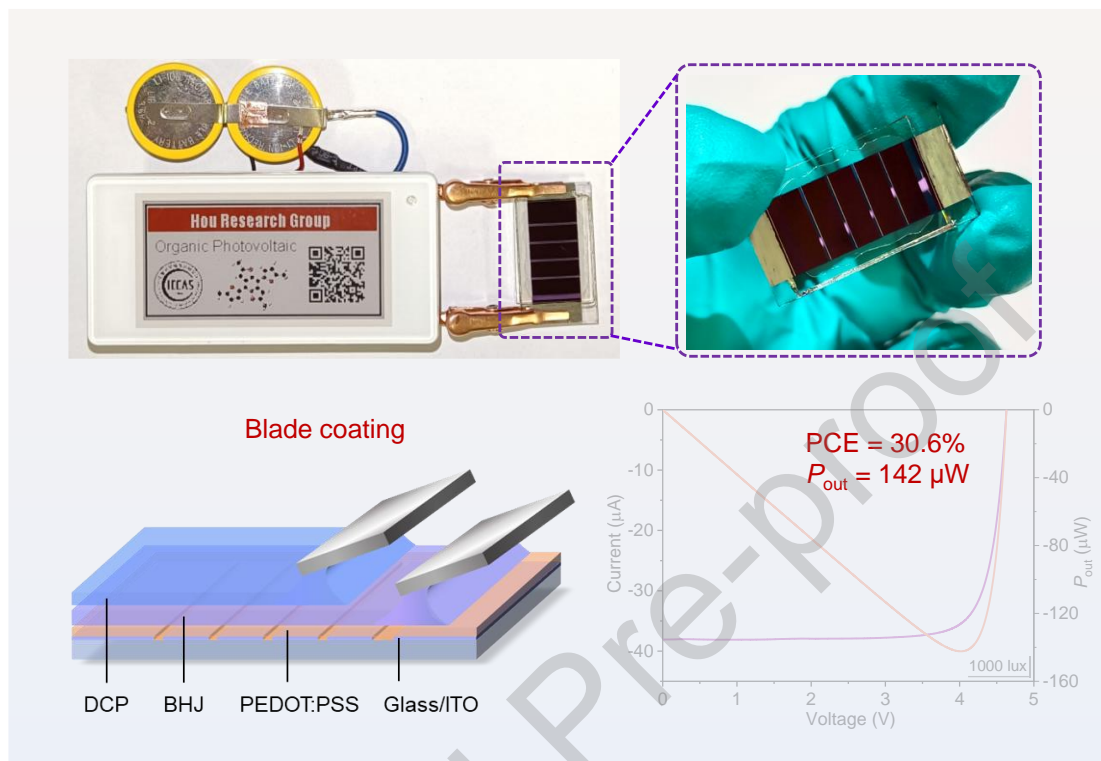
#### Declaration of interests

The authors declare that they have no known competing financial interests or personal relationships that could have appeared to influence the work reported in this paper.

The authors declare the following financial interests/personal relationships which may be

considered as potential competing interests:

### Graphical abstract



In this work, we designed and fabricated the OPV module based on the cathode interlayer DCP with thin depletion region width by blade-coating method. The module achieved a remarkable PCE of 30.6% with an output power of 142  $\mu\text{W}$  at 1000 lux. Due to the high output voltage, the module can fulfill the requirement for efficient wireless power transfer under indoor lighting.

### Highlights

- The cathode interlayer DCP exhibits thin depletion region width.
- The OPV module based on DCP achieves a remarkable PCE of 30.6% at 1000 lux.
- The DCP-based OPV cell maintains a prominent stability under indoor lighting.
- The module is successfully applied for the efficient wireless power transfer.